Matrix Biology 36 (2014) 15–27

Contents lists available at ScienceDirect

Matrix Biology

journal homepage: www.elsevier.com/locate/matbio

Structural characterization and biological properties of the amyloidogenic elastin-like peptide $(VGGVG)_3$

Pasquale Moscarelli [a], Federica Boraldi [b], Brigida Bochicchio [a], Antonietta Pepe [a], Anna Maria Salvi [a], Daniela Quaglino [b,*]

[a] Department of Sciences, University of Basilicata, Potenza, Italy
[b] Department of Life Sciences, University of Modena and Reggio Emilia, Modena, Italy

ARTICLE INFO

Article history:
Received 27 November 2013
Received in revised form 18 March 2014
Accepted 19 March 2014
Available online 28 March 2014

Keywords:
Elastin-like polypeptides
Amyloid fibrils
Supramolecular structure
Cell viability
Cell spreading
Reactive oxygen species

ABSTRACT

The peculiar and unique properties of elastin are due to the abundance of hydrophobic residues and of repetitive sequences as XGGZG (X, Z = V, L or A). Unexpectedly, these sequences not only provide elasticity to the whole protein, but are also able to form amyloid-like fibrils. Even though amyloid fibrils have been associated for a long time to the development of serious disorders as Alzheimer's disease, recent evidence suggests that toxicity may be related to oligomeric species or to pre-fibrillar intermediates, rather than to mature fibrils. In addition, a number of studies highlighted the potential of "bio-inspired" materials based on amyloid-like nanostructures. The present study has been undertaken with the aim to characterize a chemically synthesized elastin-like peptide $(VGGVG)_3$. Structural and biological features were compared with those of peptides as poly(VGGVG) and VGGVG that, having the same amino acid sequence, but different length and supramolecular structure have been previously investigated for their amyloidogenic properties. Results demonstrate that a minimum sequence of 15 amino acids is sufficient to aggregate into short amyloid-like fibrils, whose formation is however strictly dependent on the specific VGGVG repeated sequence. Moreover, in the attempt to elucidate the relationship among aggregation properties, fibers morphology and biocompatibility, 3T3 fibroblasts were grown in the presence of VGGVG-containing elastin-like peptides (ELPs) and analyzed for their ability to proliferate, attach and spread on ELPs-coated surfaces. Data clearly show that amyloid-like fibrils made of $(VGGVG)_3$ are not cytotoxic at least up to the concentration of 100 μg/ml, even after several days of culture, and are a good support for cell attachment and spreading.

1. Introduction

In the last decades, much evidence has been provided on the interesting and pleiotropic characteristics of elastin and elastin-like polypeptides. By dissecting the elastin protein, it was demonstrated that i) the entire molecule, as well as sequences of reduced size and complexity, is able to self-assemble and to reveal elastic properties (Tamburro et al., 2003; Quaglino et al., 2009); ii) mechanical and biological properties can be tuned by selecting appropriate sequences (Trabbic-Carlson et al., 2003); iii) elastin-derived peptides, depending on their sequence, are able to self-assemble into classical elastin-like (Bellingham et al., 2003) or amyloid-like (Flamia et al., 2004; Tamburro et al., 2005) structures. Due to these peculiar features, elastin and elastin-like peptides are promising bio-nanomaterials with "smart" behavior (Rodriguez-Cabello, 2004; Channon and MacPhee, 2008) in terms of structural plasticity and mechanical stability.

Within this context, there are studies proposing that amyloid fibrils, due to their unique properties (i.e. easy production, low cost, outstanding mechanical stability and remarkably regular architecture) can be used as bio-inspired nanomaterials (Lashuel et al., 2000; MacPhee and Dobson, 2000; Cherny and Gazit, 2008; Mankar et al., 2011) suitable for developing nanowires for the electronics industry as well as biosensors and functionalized supports favoring cell attachment or differentiation (Yoshiike et al., 2007; Cherny and Gazit, 2008; Gras et al., 2008; Ohga et al., 2009; Cinar et al., 2012).

In support of the proposed biocompatibility of amyloid-like fibrils are the observations indicating that the primary cause of cytotoxicity is represented by pre-fibrillar aggregates, even from non-pathogenic proteins (Bucciantini et al., 2002, 2004), rather than the initial monomers and/or the insoluble fibrils. Even though mature fibril formation and aggregation into plaques were proposed to represent a protective mechanism to avoid the high intrinsic toxicity of oligomers or of pre-fibrillar intermediates (Bucciantini et al., 2002, 2004; Caughey and

* Corresponding author at: Dept. Life Sciences, Via Campi 287, 41125 Modena, Italy. Tel.: +39 059 2055418; fax: +39 059 2055426.
E-mail address: daniela.quaglino@unimore.it (D. Quaglino).

http://dx.doi.org/10.1016/j.matbio.2014.03.004

Lansbury, 2003; Sörgjerd et al., 2008), nevertheless, examples of toxicity associated with fibrils are present (Novitskaya et al., 2006; Gharibyan et al., 2007; Pieri et al., 2012). Therefore several issues concerning the toxicity of amyloidogenic molecules still remain unanswered.

Previous studies have shown that it is possible to synthesize elastin-like amyloidogenic peptides that share the presence of the XGGZG (where G is glycine whereas X, Z can be V = valine, A = alanine, L = leucine) motif along the sequence (Tamburro et al., 2005, 2010). Consistently, it has been demonstrated that the poly(VGGLG) and poly(VGGVG) synthetic polymers obtained by the poly-condensation of the XGGZG monomer (Flamia et al., 2004; Del Mercato et al., 2008) exhibit an amyloidogenic behavior.

In the present study we have chemically synthesized and characterized a small peptide containing a 3-fold repeated motif VGGVG with the aim to confirm the hypothesis that: i) this short and specific sequence is necessary and sufficient to self-assemble into amyloid-like fibrils; ii) the population to which the fibrils belong is more homogeneous compared to those previously described; and iii) the $(VGGVG)_3$ peptide positively interacts with cells. Moreover, a further goal of the present study was to assess the toxicity of VGGVG polymers, if any, depending on the supramolecular organization of the peptide. Therefore, comparison has been also made among different VGGVG-containing elastin-like peptide (ELPs) as the newly synthesized $(VGGVG)_3$ and the amyloidogenic poly(VGGVG) polymer and the soluble pentapeptide VGGVG, which have been already characterized (Flamia et al., 2005).

The $(VGGVG)_3$ peptide was structurally characterized at molecular level by circular dichroism (CD), nuclear magnetic resonance (NMR), and Fourier transform infrared (FTIR) spectroscopy and, at supramolecular level, by atomic force microscopy (AFM), transmission electron microscopy (TEM) as well as thioflavin-T (ThT) and Congo red (CR) assays (Nilsson, 2004). Furthermore, cell viability including intracellular ROS content, as well as cell attachment and spreading on ELPs-coated surfaces were evaluated on mouse 3T3 fibroblasts. Additionally, attachment/spreading assays, CD and TEM were carried out on the scrambled peptide VVVGGGGVGVGVGGG (VGs) as control peptide in order to distinguish general effects of hydrophobic peptides versus the specific sequences that have been tested.

2. Results

2.1. CD spectroscopy

Fig. 1A shows CD spectra of the $(VGGVG)_3$ peptide recorded in aqueous solution at different temperatures. At 0 °C a negative and a positive band were centered at 218 and 200 nm, respectively, indicating a distorted beta-sheet together with unordered conformations (Manning et al., 1988). The increase of the temperature to 25 and 70 °C induces a slight decrease of the two bands due to the destabilization of beta-sheet conformation. Fig. 1B shows the CD spectra in aqueous solution of the VGs peptide. At 0 °C a strong negative band at 195 nm is visible together with a shoulder at 218 nm. These spectral findings are indicative of the presence of PPII conformation even if the expected positive band at 215 nm is absent. On increasing the temperature to 25 and 70 °C the reduction and the red shift of the negative band is observed together with the appearance of a small negative band centered at 218 nm. This finding is indicative of a conformational transition toward more folded conformations such as beta-turns. The temperature-induced folding of the peptide is probably due to hydrophobic interactions. For the evaluation of secondary structure content, analysis of CD spectra was performed with DICHROWEB analysis webserver (Whitmore and Wallace, 2008) using

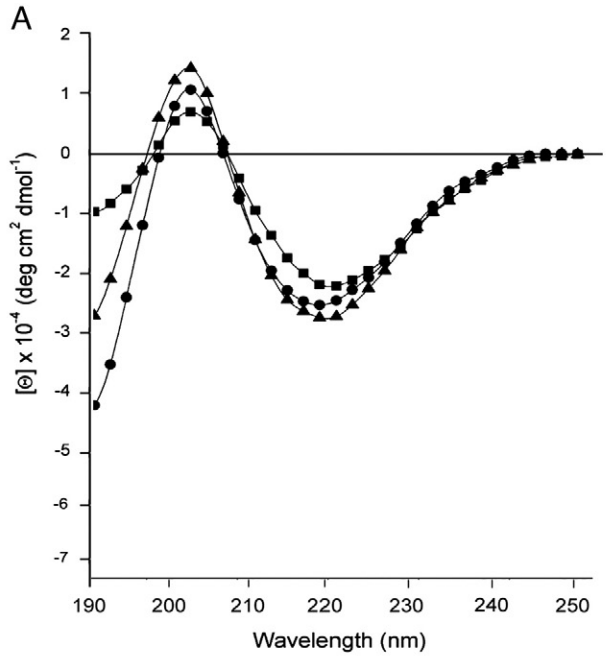

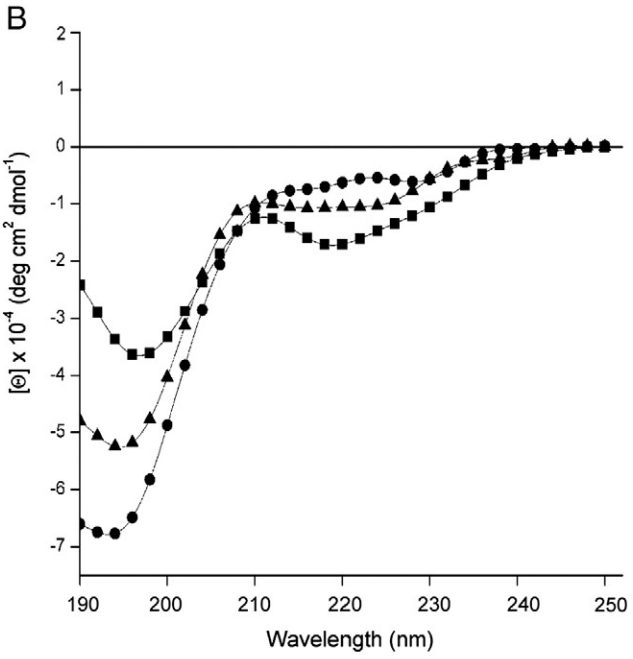

C

Temperature	Helix	Strand	Turn	Unordered
0°C	5	37	23	35
25°C	3	39	27	31
70°C	3	43	21	33

D

Temperature	Helix	Strand	Turn	Unordered
0°C	5	30	17	48
25°C	5	31	17	47
70°C	5	32	18	46

Fig. 1. Secondary structure analysis by circular dichroism (CD) spectroscopy. CD spectra of the $(VGGVG)_3$ peptide (A) and the VGs scrambled peptide (B) have been acquired in aqueous solution at temperature of 0 °C (circle), 25 °C (triangle), 70 °C (square). Tables show results of the deconvolution algorithm CONTINLL for secondary structure calculations applied to CD spectra of $(VGGVG)_3$ (C) and VGs peptides (D).

the CONTINLL algorithm (showing the best fit among different available algorithms) (Provencher and Glockner, 1981). Results indicate a predominance of beta-sheet and of unordered conformations for $(VGGVG)_3$ and VGs, respectively (Fig. 1C and D).

2.2. NMR spectroscopy

Conformational analyses of the $(VGGVG)_3$ peptide (Fig. 2A) were performed in H_2O/D_2O (90/10, v/v) (Fig. 2B) and in DMSO-d_6, an aprotic organic solvent that prevents aggregation (Fig. 2C). Through standard procedures (Wüthrich, 1986), the chemical shifts, the temperature coefficients (Δδ/ΔT, ppb/K) of the amide protons, $^3J_{NH-H\alpha}$ coupling constants and NOE connectivities have been investigated (Tables 1 and 2).

In H_2O/D_2O (90/10, v/v) the evaluation of the Hα proton chemical shifts was in the range that is generally assigned to random coil conformation, excluding the presence of significant amount of α-helix, or β-sheet structures (Table 1) (Wishart et al., 1992). The analysis of the temperature coefficients showed values between 6.4 and 7.9 ppb/K, usually ascribed to amide protons not shielded from the solvent. However, the $^3J_{NH-H\alpha}$ coupling constants of some valine residues was around 8.2–9.0 Hz, that could infer φ dihedral angles of −95°, −145° compatible with more extended conformations, such as β-strands. Also the analysis of the NOE pattern in the amide region showed the presence of small sequential d_{NH-NH} NOEs consistent with random-coil/β-strand structures. Some more intense NOEs were observed only for the overlapping $V_{1'}$–$G_{2'}$, $V_{1''}$–$G_{2''}$ and $G_{2'}$–$G_{3'}$ and $G_{2''}$ and $G_{3''}$ d_{NN} cross-peaks.

Table 1
Assignments of proton resonances of peptide $(VGGVG)_3$ in H_2O/D_2O(90/10, v/v) at 25 °C.

Residue[a]	Chemical shift (ppm) NH	Hα	Hβ	Hγ	$^3J_{NH-H\alpha}$ (Hz)	−Δδ/ΔT (ppb/K)
V^1	–	3.87	2.24	1.08/1.02	–	–
G^2	8.77	4.05			12.4	6.9
G^3	8.39	3.99			12.6	6.7
V^4	8.11	4.16	2.11	0.93	8.2	6.8
G^5	8.54	3.98			12.6	6.8
$V^{1'}$	8.05	4.14	2.11	0.93	7.3	7.7
$G^{2'}$	8.58	3.97			12.6	7.9
$G^{3'}$	8.24	3.97			nd	nd
$V^{4'}$	8.03	4.14	2.14	0.93	8.2	6.2
$G^{5'}$	8.52	3.98			12.6	6.7
$V^{1''}$	8.04	4.15	2.11	0.93	7.3	7.7
$G^{2''}$	8.58	3.97			12.6	7.9
$G^{3''}$	8.24	3.97			nd	nd
$V^{4''}$	8.00	4.21	2.14	0.94	9.0	6.5
$G^{5''}$	8.26	3.87			nd	6.4

[a] The J values for Gly residues are the sum of J_{AX} and J_{BX}.

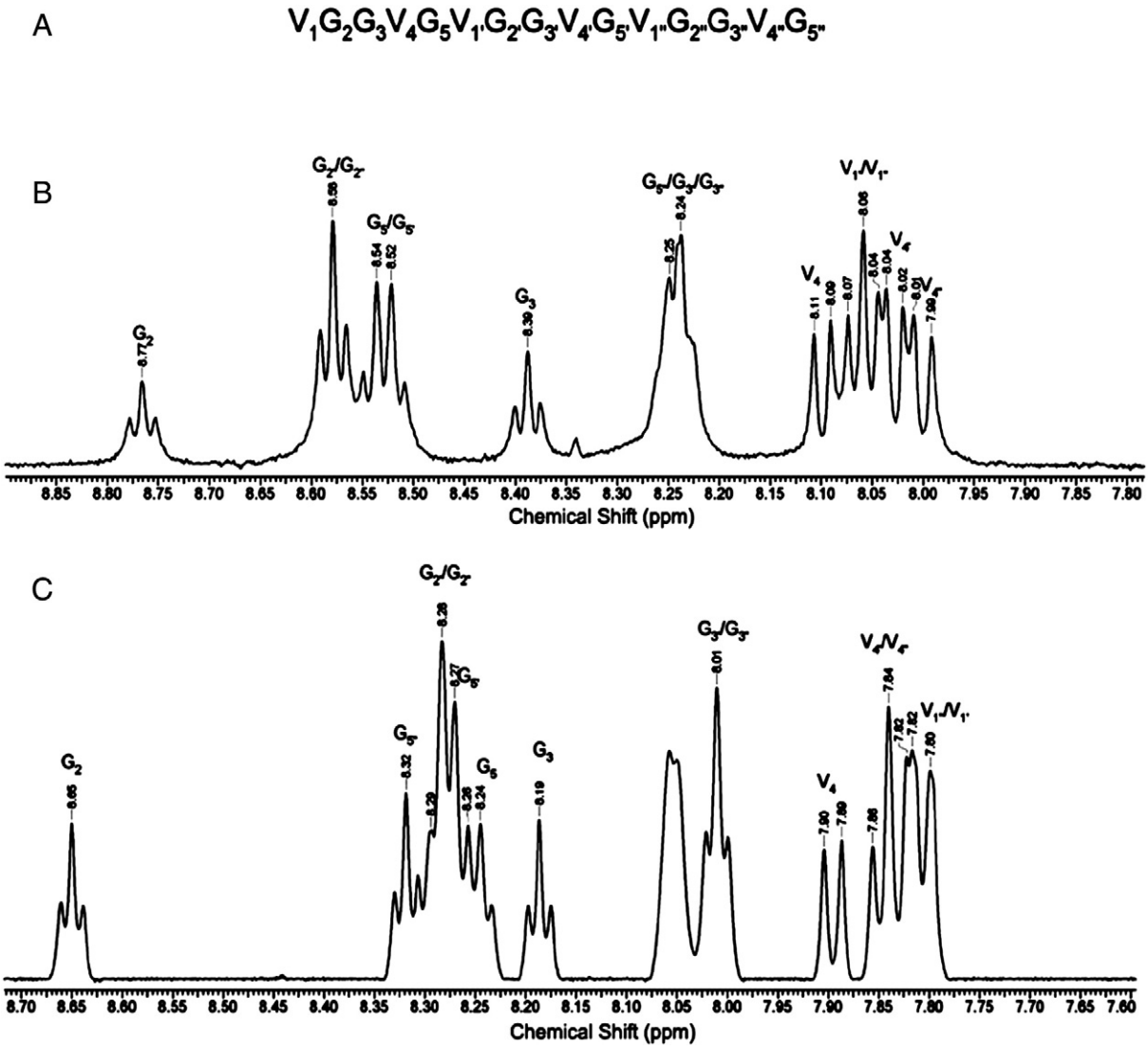

Fig. 2. Residues numbering scheme of the $(VGGVG)_3$ peptide (A) and ^1H NMR spectra of the amide region recorded in (B) H_2O/D_2O (90/10, v/v) and (C) DMSO-d_6 at 25 °C.

Table 2
Assignments of proton resonances of peptide $(VGGVG)_3$ in DMSO-d_6 at 25 °C.

Residue[a]	Chemical shift (ppm)				$^3J_{NH-H\alpha}$ (Hz)	$-\Delta\delta/\Delta T$ (ppb/K)
	NH	Hα	Hβ	Others		
V^1	–	3.64	2.08	0.95	–	–
G^2	8.65	3.92/3.81			10.7	3.9
G^3	8.19	3.82			11.0	4.4[b]
V^4	7.89	4.18	1.97	0.85/0.83	8.6	5.2
G^5	8.24	3.81/3.73			11.0	4.6
$V^{1'}$	7.80	4.16	1.97	0.86/0.83	8.9	5.4
$G^{2'}$	8.28	3.73			nd	nd
$G^{3'}$	8.01	3.78			10.7	4.2[b]
$V^{4'}$	7.84	4.17	1.97	0.85/0.83	7.9	4.8
$G^{5'}$	8.27	3.78/3.73			12.5	nd
$V^{1''}$	7.80	4.16	1.97	0.85/0.83	9.0	5.4
$G^{2''}$	8.28	3.73			nd	nd
$G^{3''}$	8.01	3.78			10.7	4.2[b]
$V^{4''}$	7.83	4.20	1.98	0.87	nd	5.0
$G^{5''}$	8.32	3.79/3.70			11.6	5.8

[a] The J values for Gly residues are the sum of J_{AX} and J_{BX}.
[b] Solvent-shielded amide protons, possible involved in H-bound formations.

The complete chemical shift assignments of the $(VGGVG)_3$ peptide was further investigated by NMR spectroscopy in DMSO-d_6 (Table 2). The analysis of the temperature coefficients highlighted the presence of some amide protons shielded from the solvent, possibly involved in H-bond formations. In particular, the overlapping $G_{3'}$ and $G_{3''}$ show coefficient temperature values ($\Delta\delta/\Delta T$, ppb/K) of 4.2 ppb/K suggesting the presence of a significant population of conformers adopting a turn structure in the sequence $G_5VGG_{3'}$ and $G_{5'}VGG_{3''}$. Consistently, NOE analysis revealed a typical medium range NOE $d_{\alpha N(i,i+2)}$ between $V_{1'}/G_{3'}$ and $V_{1''}/G_{3''}$, together with sequential d_{NN} and $d_{\alpha N}$ NOE cross-peaks.

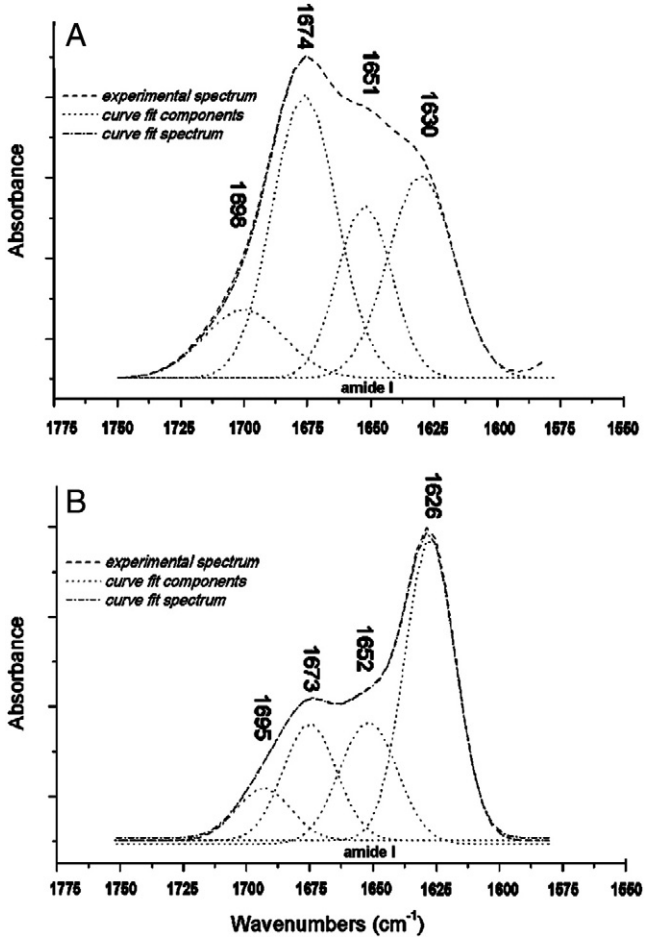

Fig. 3. Secondary structure analysis by Fourier transform infrared (FTIR) spectroscopy. Fitted FTIR spectra of the Amide I region were obtained on lyophilized powder (A) and on aggregated fibrils (B) in KBr pellet. Peaks from a Gaussian deconvolution of FTIR spectra are shown.

2.3. FTIR spectroscopy

The Amide I region of $(VGGVG)_3$ was analyzed by FTIR spectroscopy on powder (Fig. 3A) and on fibrils (Fig. 3B). Fig. 3A shows that there is a main component at 1674 cm^{-1} attributable to β-turn and/or PPII conformations (Surewicz et al., 1993; Martino et al., 2000). The additional strong component at 1630 cm^{-1} combined with a weaker one at 1698 cm^{-1} is indicative of the presence of antiparallel β-sheet conformation (Krimm and Bandekar, 1986; Barth, 2007). The remaining component at 1651 cm^{-1} is usually assigned to unordered conformations (Barth, 2007). The FTIR analysis of the Amide I region of $(VGGVG)_3$ fibrils (Fig. 3B) is similar to the previous one, being characterized by the same components described for the $(VGGVG)_3$ powder. Differences are due to the relative intensities of component's structures. The dominant component is centered at 1626 cm^{-1} and is indicative of β-sheet secondary structure. This component together with the one at 1695 cm^{-1}, is indicative of antiparallel β-sheets arranged in a cross-β structure (Krimm and Bandekar, 1986; Zandomeneghi et al., 2004; Barth, 2007). The components at 1652 cm^{-1} and 1673 cm^{-1} were assigned to unordered conformation (Barth, 2007) and to β-turn and/or PPII conformation (Surewicz et al., 1993; Martino et al., 2000), respectively. Due to the aggregation process, the peak centered at around 1630 cm^{-1} (Fig. 3A) is shifted to 1626 cm^{-1}, indicating that a C═O group is involved in strong hydrogen bonds, in agreement with the increased number of β-strands involved in the β-sheet (Zandomeneghi et al., 2004; Barth, 2007), as expected for the extremely stable structure of amyloid-like fibrils.

2.4. Time-dependent aggregation profiles of polypeptides and amyloid formation

A ThT binding assay was carried out to study the aggregation kinetics (Fig. 4) of $(VGGVG)_3$ and data were compared with those of poly(VGGVG) and of the monomer VGGVG (Fig. 5). The ThT dye specifically binds

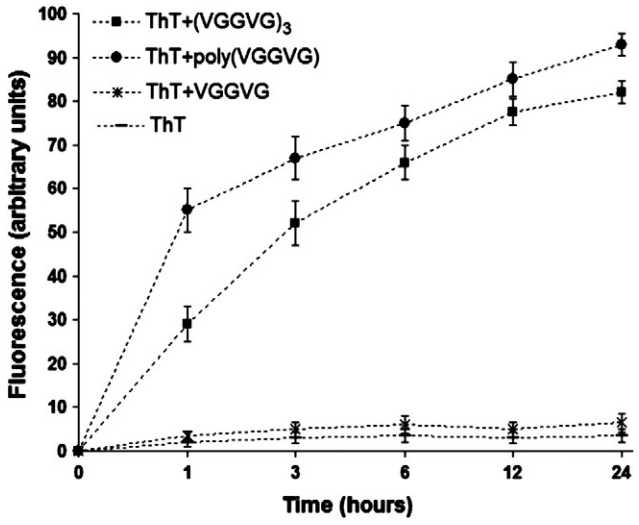

Fig. 4. Peptide aggregation kinetics by Thioflavin-T (ThT) fluorescence spectroscopy. The extent of aggregation in aqueous solution was assessed, at intervals of 1, 3, 6, 12, 24 h, at 37 °C. The behavior of the $(VGGVG)_3$ peptide was compared with that of poly(VGGVG) and of the monomer VGGVG. Data are expressed as the mean ± SD of at least three experiments.

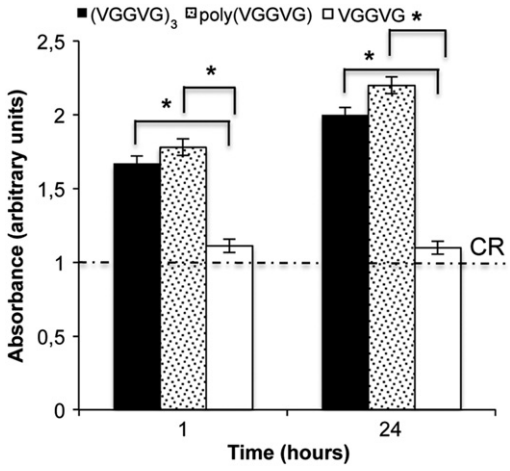

Fig. 5. Amyloid-like fibril formation by Congo red (CR) spectroscopic assay. Fibril formation in aqueous solution was evaluated after 1 hour- and 24 hour-incubation at 37 °C by CR binding. The behavior of the $(VGGVG)_3$ peptide was compared with that of poly(VGGVG) and of VGGVG. Data have been normalized to CR background set at 1 and are expressed as the mean ± SD of at least three experiments. $^*p < 0.05$.

to β-sheet structures, which are characteristic of amyloid-like fibrils, producing a shift in the emission spectrum and a fluorescent signal proportional to the β-sheet content (LeVine, 1999; Nilsson, 2004).

In Fig. 4, the aggregation kinetics in aqueous solution of $(VGGVG)_3$ and of poly(VGGVG) show an exponential growth phase, characteristic of a nucleation-dependent polymerization and typical of amyloid fibril formation (Nilsson, 2004). A lag phase was not evident probably because of the temperature-induced increase of the aggregation rate. As incubation time increased, there was an increase in ThT fluorescence for the poly(VGGVG) and the $(VGGVG)_3$ (Fig. 4). On the contrary, reduction of the polypeptide sequence to the monomer VGGVG completely abolished the ability of the peptide to aggregate. A similar kinetic was observed when polypeptide aggregation was evaluated by measuring the increase in solution's turbidity (data not shown).

Moreover, our recent studies have shown a strong dependence of the supramolecular structure of the poly(VGGVG) on the specific solvent used for polymer solubilization (Salvi et al., 2013) and therefore ThT measurements were also performed in a 50% DMSO–water solution. DMSO has been in fact shown to inhibit or completely dissociate amyloid fibrils based on its ability to disrupt a hydrogen bond network (Loksztejn and Dzwolak, 2009). Consistently, the ThT fluorescence intensity of each polypeptide in 50% DMSO–water solution rapidly decreases to values close to those of the unassembled VGGVG and of free ThT (data not shown).

Amyloid-like fibril formation in aqueous solution was further evaluated with the CR binding assay (Fig. 5). As expected, VGGVG did not bind to CR, as demonstrated by absorption values at 540 nm similar to basal levels (CR). By contrast, absorption values were significantly increased compared to VGGVG when CR was incubated with the $(VGGVG)_3$ or with the poly(VGGVG) polymer.

2.5. Supramolecular organization

The supramolecular organization of $(VGGVG)_3$ was investigated by AFM in different environmental conditions, i.e. in the presence of DMSO and in aqueous solution. Results were compared with those of poly(VGGVG) and of the monomer VGGVG.

In the presence of DMSO all ELPs were inhibited to form aggregates and/or fibrils (Fig. 6), even after several hours of incubation at 37 °C (data not shown).

By contrast, already after 1 h of incubation in aqueous solution at 37 °C, both $(VGGVG)_3$ and poly(VGGVG) formed fibrils of variable width and length. These fibrils increased in size with time, as shown after 24 h of incubation at 37 °C (Fig. 6). To be noted that in the case of $(VGGVG)_3$ fibrils were smaller and more homogeneous compared to those formed by poly(VGGVG) (Fig. 6). The monomer VGGVG never gives rise to fibrillar structures and, at 24 h, only small round aggregates were observed (Fig. 6).

Ultrastructural observations of negatively stained ELPs confirmed AFM analyses and allowed to further investigate the supramolecular organization of amyloid-like fibrils. As shown in Fig. 7, $(VGGVG)_3$ formed short amyloid-like fibrils organized in a "snowflake" model in which fibrils arise from an electrondense nucleation core (Fig. 7A and B). This peculiar morphology is rather stable, since it was observed after several days of incubation of the peptides in the aqueous solution at 37 °C (data not shown). Compared to the $(VGGVG)_3$, the poly(VGGVG) formed longer and thicker fibrils with a waving appearance possibly due to heterogeneous assembly of a variable number of molecules (Fig. 7D). By contrast, the monomer VGGVG was only able to form small round aggregates and fibrils of any size were never observed (Fig. 7E). To elucidate if the repeated VGGVG sequence is necessary to form amyloid-like fibrils, a VGs scrambled peptide was investigated. As shown in panel C, this peptide was organized in globular structures forming large aggregates in the absence of fibrils.

2.6. Cell viability and cell morphology

In order to assess if $(VGGVG)_3$ amyloid-like fibrils exert cytotoxic effects on 3T3 fibroblasts, cells were cultured in the presence of ELPs, as described in the experimental procedures. Data were compared with those obtained in the presence of poly(VGGVG) and VGGVG.

All peptides did not affect cell proliferation, as evaluated by counting the cell number up to 48 h from seeding in the presence of ELPs. After 48 h of culture, at concentrations higher than 100 μg/ml, there was a dose-dependent increase in cell death (Fig. 8A). These effects were independent from the supramolecular organization of ELPs (also the monomer that did not form fibrillar structures appeared cytotoxic), and from changes in the intracellular ROS content (Fig. 8C–D). Consistently, the monomer VGGVG never increased the ROS content, even at doses that affected cell proliferation. By contrast, although only at the highest dose, poly(VGGVG) induced a significant increase of $O_2^{-\bullet}$, whereas $(VGGVG)_3$ caused a significant raise of H_2O_2.

Looking at the morphology of cells at doses that did not affect cell proliferation, it appeared that 3T3 fibroblasts formed an ordered monolayer comprising of cells with a typical elongated shape (Fig. 8B).

2.7. Cell attachment and spreading assay

3T3 fibroblasts showed a variable attachment to the surfaces coated with different ELPs (Fig. 9). Compared to the positive control (i.e. cells on tissue culture plates), fibroblasts on fibrillar $(VGGVG)_3$-coated surfaces displayed very similar attachment values ($p = ns$). Cells seeded on the surface coated by the VGs peptide exhibited highest attachment values ($p < 0.05$). By contrast, attachment of 3T3 cells on the fibrillar poly(VGGVG)-coated surfaces was significantly lower ($p < 0.05$) compared to $(VGGVG)_3$, but significantly higher compared to the monomer VGGVG ($p < 0.05$). No significant differences ($p = ns$) were seen between VGGVG-coated and uncoated surfaces, values being consistently lower ($p < 0.05$) compared to other ELPs. As expected, BSA-coated plates inhibited cell attachment.

Cell spreading up to 24 h is visualized in Fig. 10. Looking at the morphology of cells spread on the different surfaces, it appeared that on BSA-coated surfaces and on uncoated dishes the few attached cells were small and round even after several hours. By contrast, cells seeded on tissue culture plates (i.e. positive control), as well as on fibrillar $(VGGVG)_3$-coated surfaces, show a flattened morphology. Cells on fibrillar poly(VGGVG) displayed an intermediate morphology between that seen for adherent cells on $(VGGVG)_3$ and on the monomer VGGVG. Unexpectedly, despite good adhesive properties, cells plated

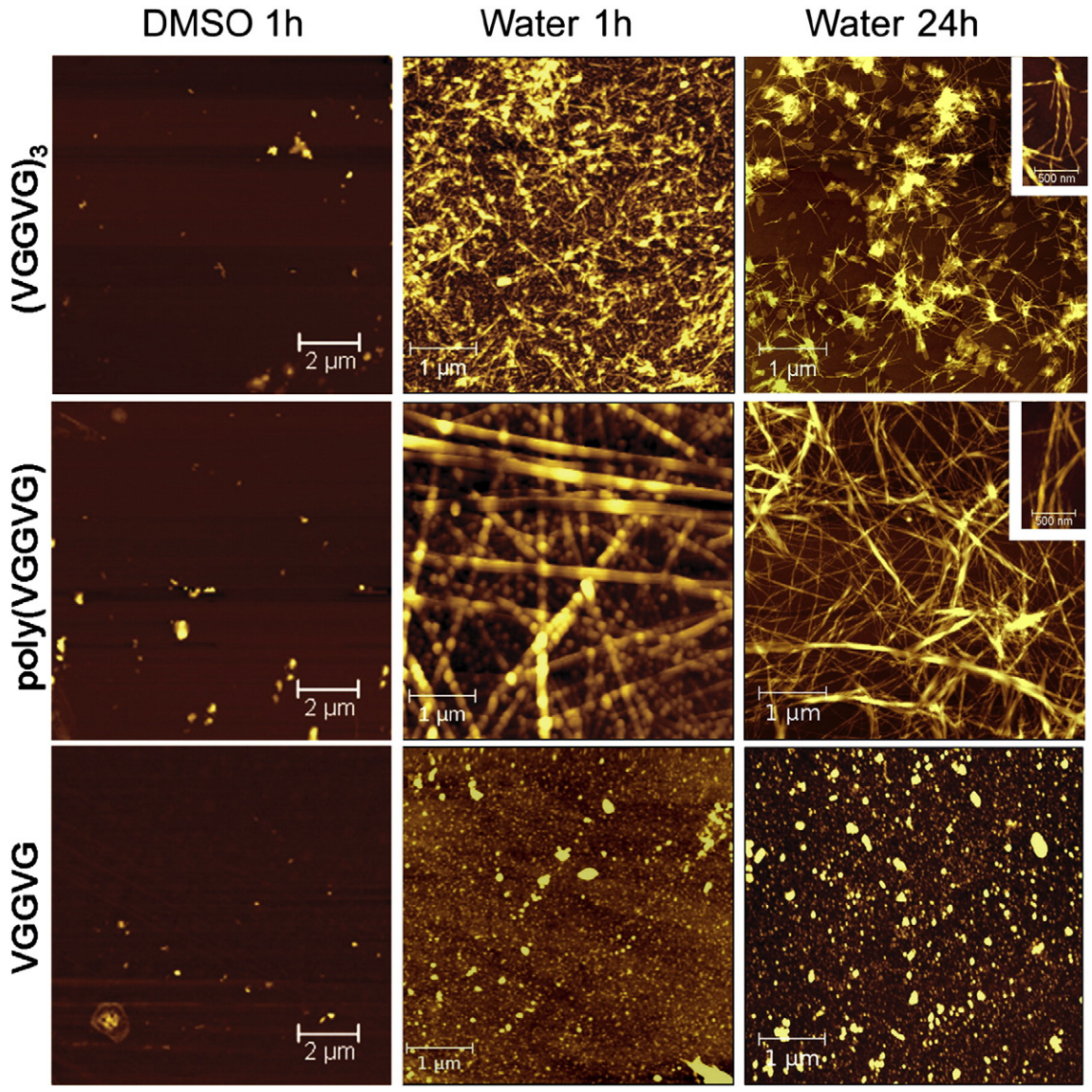

Fig. 6. Analysis of supra-molecular organization by atomic force microscopy (AFM) of $(VGGVG)_3$, poly(VGGVG) and VGGVG. Observations were performed on peptides dissolved in DMSO or suspended in water and incubated at 37 °C. In water, both $(VGGVG)_3$ and poly(VGGVG) self-assemble into amyloid-like fibrils, compared to the monomer VGGVG that forms only amorphous aggregates. As expected, peptides in DMSO never showed fibrillar structures. Representative images on silicon substrate are shown.

on surfaces coated with VGs were characterized by the presence of numerous cytoplasmic vacuoles. In addition, these cells exhibited a very heterogeneous size at early time points, whereas they acquired a spindle-shaped structure at 24 h after seeding.

In order to verify if cells effectively adhere to fibrillar structures and not to empty spaces between fibrils, cell cultures were stained with Congo red (for amyloid-like fibrils) and ferric-haematoxylin (for cells). A CR positive staining was only observed in the case of fibrillar aggregates produced by $(VGGVG)_3$ and poly(VGGVG), while the monomer VGGVG did not show any CR binding. Fig. 11 reveals that, after 24 h of culture, the few cells on the VGGVG monomer are round with little evidence of spreading, while those on both $(VGGVG)_3$ and poly(VGGVG) coated surfaces are nicely spread along the fibrils.

3. Discussion

Amyloid and amyloid-like fibrils are insoluble, stable and ordered polymers that can be formed in vitro from a broad range of soluble proteins and peptides of different sequence and length. Even though spectroscopic studies have shown that amyloid formation is highly sequence- and environment-dependent (Kelly, 1998; Dobson, 1999), amyloidogenic proteins share similar conformational features (Kelly, 1998; Dobson, 1999), being predominantly composed of β-sheet structure in a characteristic cross-β-sheet conformation (Sunde et al., 1997). The highly ordered arrangement of side-chains within fibrillar structures implies an important role for side-chain interactions in the molecular recognition events leading to self-assembly and in the stabilization of the final amyloid structures, although, at present, the precise mechanisms of peptide self-assembly are still under investigation.

Among the proteins which are able to self-assemble, there are a number of elastin and elastin-like peptides forming amyloid-like fibrils sharing the presence of the XGGZG motif along the sequence (Flamia et al., 2004; Tamburro et al., 2005; Del Mercato et al., 2008; Tamburro et al., 2010).

On the basis of previous experimental data on ELPs containing the VGGVG sequence, i.e. poly-(VGGVG) and the VGGVG monomer (Flamia et al., 2005), we have performed a structural and biological characterization of the peptide $(VGGVG)_3$ as a potential good candidate for developing bio-inspired nanomaterials (Rodriguez-Cabello, 2004; Channon and MacPhee, 2008). Polypeptide molecular weight control

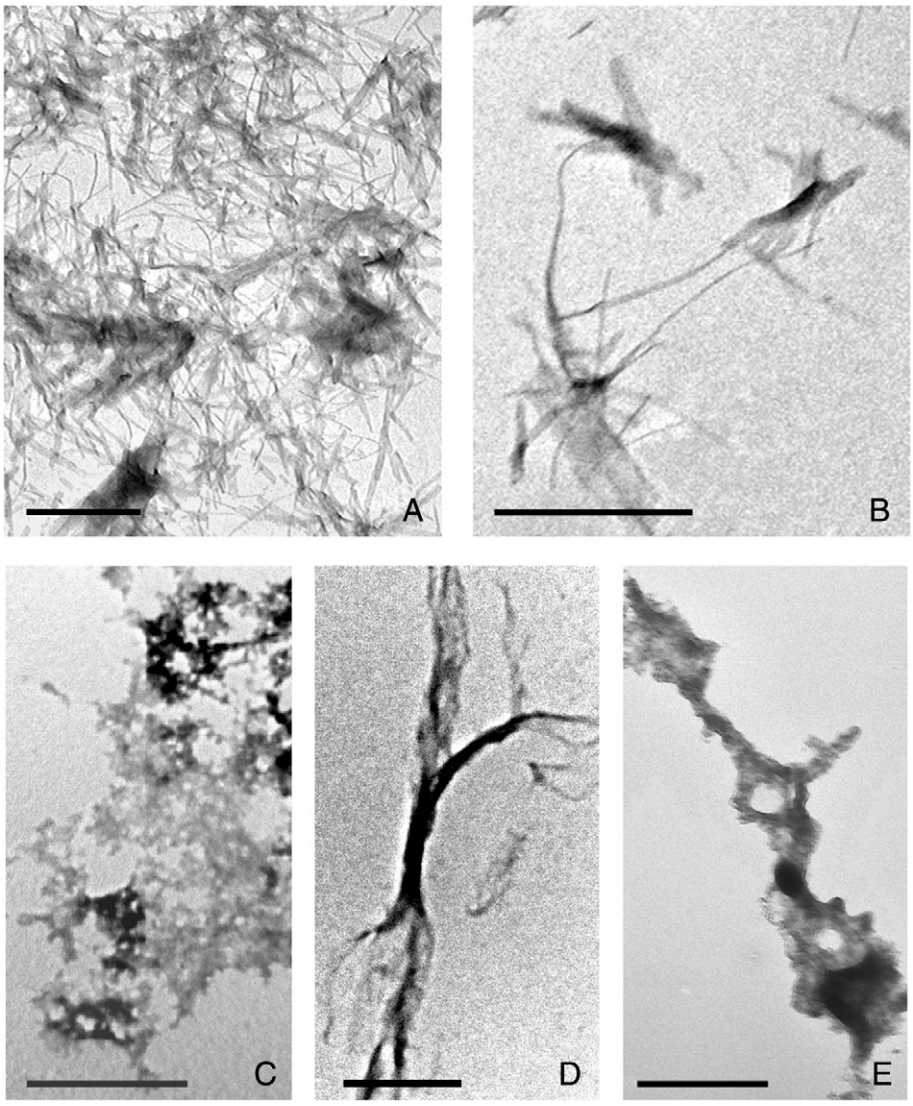

Fig. 7. Analysis of the supramolecular organization by transmission electron microscopy (TEM) of $(VGGVG)_3$, poly(VGGVG), VGGVG and of the VGs scrambled peptide. Observations were performed after negative staining of peptides incubated in water for 24 h at 37 °C. Both $(VGGVG)_3$ (A–B) and poly(VGGVG) (D) self-assemble into amyloid-like fibrils, compared to the monomer VGGVG (E) and the VGs peptide (C), which form only amorphous aggregates. Panel B shows at higher magnification the peculiar structure and organization of $(VGGVG)_3$ fibrils. Scale bars = 1 μm.

is mandatory for the proper design of tailored nanostructured materials. Aim of this study was the characterization of the $(VGGVG)_3$ peptide that, being synthesized by solid phase peptide synthesis, has a monodispersed molecular weight. Due to this property, the $(VGGVG)_3$ shows an advantage over the previously described poly(VGGVG) that, on the contrary is obtained by poly-condensation reactions and is characterized by a mixture of peptides of different length.

Results demonstrate that the $(VGGVG)_3$ peptide self-assembles and that during the aggregation process it adopts a β-conformation. NMR data recorded in aqueous solution, in agreement with CD results, show that, in the $(VGGVG)_3$ peptide, β-strands coexist with random coil conformation. Moreover, from FTIR spectra, the position of the dominant peak found at 1626 cm^{-1} is close to that observed for poly(VGGVG) fibrils at 1617–1635 cm^{-1} (Salvi et al., 2011), which is also indicative of cross-β-sheet structure. All together, FTIR data show that the antiparallel β-sheet is the main structural component of $(VGGVG)_3$ fibrils, whereas in the lyophilized powder it exerts a minor contribution because of the coexistence of PPII, β-turns and unordered conformations. Subtle differences in peak position for both $(VGGVG)_3$ and poly(VGGVG) fibrils are suggestive for the occurrence of small variations in polypeptide packing.

The hypothesis that fibril formation depends not only on the amino acid sequence, but also on the ability to form supramolecular structures (i.e. peptide length), is supported by results from ThT measurements indicating that the monomer VGGVG never forms amyloid-like fibrils and that in the presence of the polar solvent DMSO, that destroys the hydrogen bond network (Lokstejn and Dzwolak, 2009), amyloid-like fibrils are completely dissociated and/or inhibited (Salvi et al., 2013).

Consistently, AFM and TEM analyses of fibrillar preparations confirm that $(VGGVG)_3$ self-assembles into short amyloid-like fibrils with a peculiar and rather homogeneous array, in contrast to poly(VGGVG) that gives rise to intertwined and elongated fibrils. As expected, the monomer VGGVG only forms amorphous aggregates without any trace of fibrillar structures.

The morphology of $(VGGVG)_3$ fibrils was consistent between different preparations and was maintained in vitro for several days in the aqueous environment, confirming that a length of 15 amino acids is sufficient to form amyloid-like fibrils and, most importantly, the formation of these fibrils is dependent on the specific repeated VGGVG sequence, as it was demonstrated by investigating the VGs scrambled peptide that is unable to form fibrils of any type. At molecular level, CD studies highlight remarking structural differences between the $(VGGVG)_3$ and

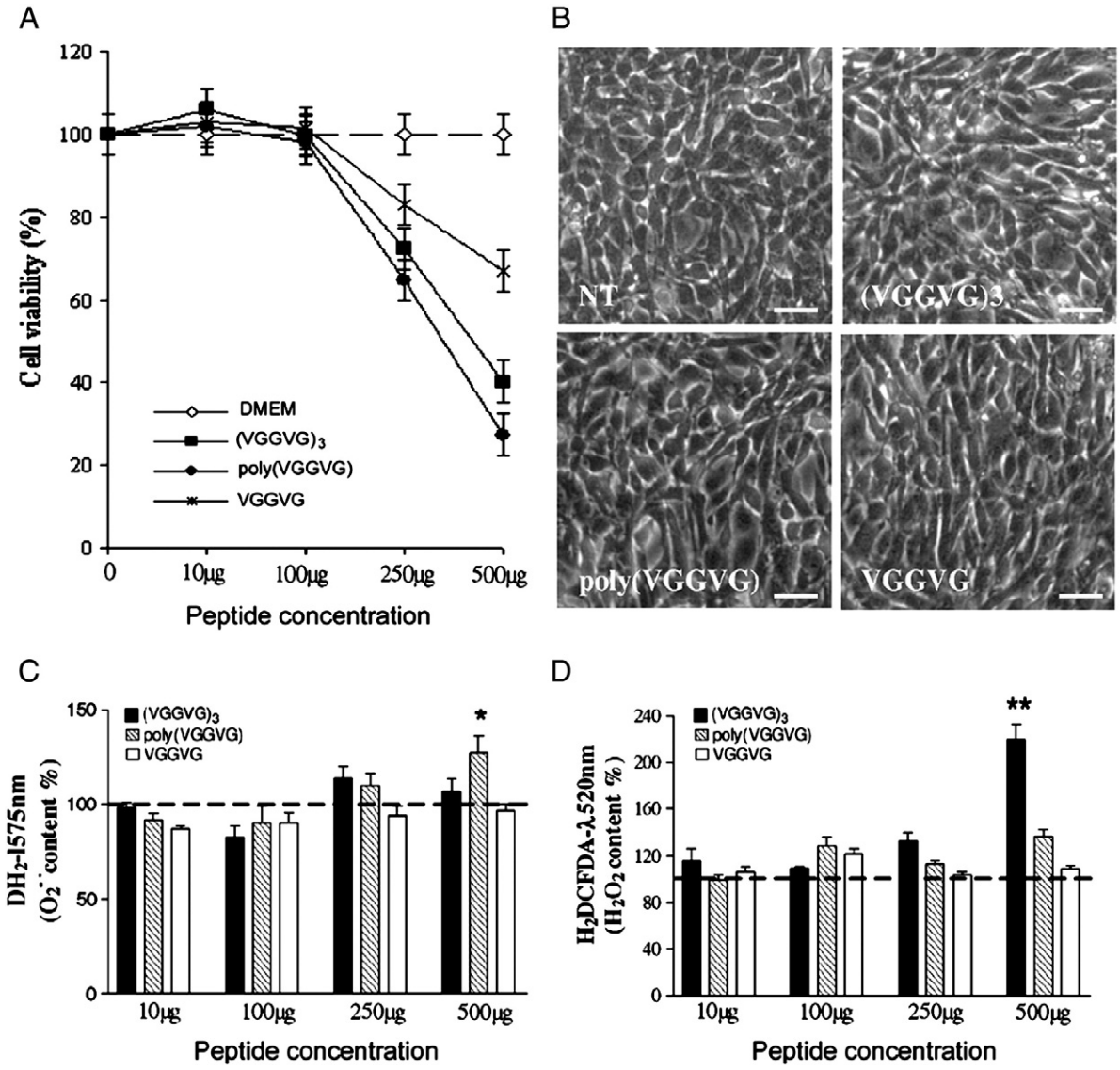

Fig. 8. Viability and morphology of 3T3 fibroblasts. Cell were cultured in DMEM alone or supplemented with different concentrations of $(VGGVG)_3$, poly(VGGVG) and VGGVG. A) As an indicator of cell viability, cell number was measured after 72 h from seeding and values from cells cultured in the presence of ELPs were expressed as percentage of the number of cells grown in DMEM alone set at 100%. Data represent the mean ± SD of three experiments done in duplicate. B) The morphology of cells grown for 72 h in the presence of 100 μg/ml of each peptide was evaluated by a phase contrast inverted microscope. Images are representative of at least three experiments, bars = 50 μm. C) Reactive oxygen species (ROS) analysis in 3T3 fibroblast cells exposed for 1 h to different concentrations of ELPs. Intracellular ROS levels were evaluated by flow-cytometry using the fluorescent probes DH_2 and H_2DCF-DA, which detect superoxide anion and hydrogen peroxide, respectively. Histograms represent the mean fluorescence intensities, expressed as percentage ± SD of three experiments done in duplicate, in cells exposed to increasing concentrations of fibrillar peptides, compared to cells grown in DMEM alone (dashed line) set at 100%. *$p < 0.05$; **$p < 0.01$.

the VGs that adopts mainly extended/unordered conformations. Values of width of the fiber and pitch of the twist in $(VGGVG)_3$ fibrils range from 6 to 15 nm and 40 to 60 nm, respectively, whereas poly(VGGVG) fibrils are substantially thicker being characterized by a distribution of size ranging from 50 to 100 nm in width and up to several microns in length. In agreement with previous AFM findings, greater thickness and size heterogeneity, as that of poly(VGGVG) fibrils, appear to be due to further interactions and supercoiling of different fibrils, which produce densely packed assemblies whose thickness is a multiple of 60 nm (Flamia et al., 2007). Since experimental evidences indicate that oligomeric precursors or prefibrillar aggregates, rather than initial monomers and final insoluble fibrils, may be the primary cause of cytotoxicity (Kayed et al., 2003; Cleary et al., 2005), we have investigated cell viability and cell-peptide interactions of 3T3 fibroblasts cultured in the presence of $(VGGVG)_3$ fibrils.

Cell morphology as well as cell proliferation was never affected by the ELPs, up to a concentration of 100 μg/ml. The toxicity observed after several days of culture at higher doses was not caused by the presence of contaminant residues, as demonstrated by appropriate tests after peptide synthesis, and was independent on the supramolecular organization of ELPs, since no significant differences were observed between $(VGGVG)_3$, poly(VGGVG) and the monomer VGGVG. Therefore, toxicity could be due to the interactions of these peptides with cell membranes, these effects being dependent on peptide concentrations and/or the structure of specific peptide regions (Tofoleanu and Buchete, 2012). However, in order to further assess the biocompatibility of fibrillar polypeptides, the intracellular content of ROS was also evaluated, as it has been shown that oxidative stress could represent one of the earliest biochemical modification in cells exposed to amyloid aggregates (Butterfield et al., 2001; Bucciantini et al., 2004; Tabner et al., 2005; Cecchi et al., 2007). Nevertheless, a growing number of in vitro and in vivo evidence showed that the redox imbalance, observed in several neurodegenerative diseases and attributable to an overproduction of reactive oxygen species (ROS) (Butterfield et al., 2001; Bucciantini et al., 2004; Tabner et al., 2005; Cecchi et al., 2007), may actually arise preferentially during fibril formation rather than in

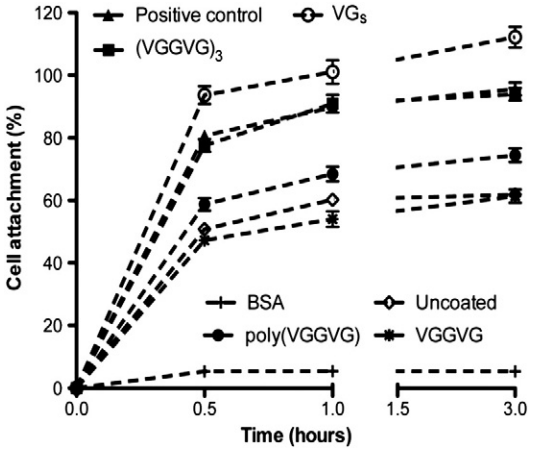

Fig. 9. Attachment of 3T3 fibroblasts. Cells were cultured in the absence of serum on bacteriologic Petri dishes coated with 100 μg/ml of $(VGGVG)_3$, poly(VGGVG), VGGVG and the VGs scrambled peptide. Dishes uncoated or coated with BSA (negative control) or tissue culture dishes (positive control) were taken as additional reference parameters. At each time point, the number of adherent cells was assessed by spectrophotometric reading of the crystal violet released by stained cells. Values are expressed as the percentage of attached cells normalized to the highest attachment value obtained in each experiment. Data represent the mean ± SD of at least two experiments done in duplicate.

the presence of mature and stable fibrillar structures. Present data indicate that the cytotoxicity observed at the highest concentrations of fibrillar peptides, is associated to increased levels of hydrogen peroxide and/or of anion superoxide. It is unclear however, if these changes are the consequence of membrane damages induced by the interactions of peptides with cell membranes, as previously hypothesized (Tofoleanu and Buchete, 2012), or the cause of cell death.

Therefore, VGGVG containing peptides, also in the fibrillar form, can be regarded as biocompatible molecules, at least up to the concentration of 100 μg/ml.

As a potential candidate for bio-inspired biomaterials, the $(VGGVG)_3$ peptide must also optimally interact with cells. Hence, attachment and spreading of cells on ELPs-coated surface were evaluated on 3T3 fibroblasts. Results demonstrate that the $(VGGVG)_3$ peptide represents a good substrate for cell attachment and spreading, since cell behavior overlaps that observed by cells cultured on tissue culture plates used as positive control. However, poly(VGGVG), despite its fibrillar structure, induced a reduced cell attachment compared to $(VGGVG)_3$ possibly due to additional interactions leading to supercoiling of individual fibrils and to increased lateral association among fibrils (as observed by AFM and TEM).

By contrast, the monomer VGGVG and the VGs scrambled peptide, although are both unable to form fibrillar structures, exhibit a different cellular response. Despite the good adhesive properties of the scrambled peptide, cells seeding on VGs are characterized by a rapid accumulation of cytoplasmic vacuoles and, at 24 h after plating, exhibit a shrunk spindle-shape appearance. In contrast, monomer VGGVG causes a decrease in the number of attached and spread cells. Therefore, in the absence of amyloid-like fibril formation, differences in cell attachment and spreading could be due to the hydropathy index of two peptides (29.2 and 9.6 for VGs and VGGVG, respectively) (Kyte and Doolittle, 1982). However, the hydropathy index cannot explain the different behavior of cells plated on VGs and $(VGGVG)_3$. These two peptides, having identical amino acid content, yield the same hydropathy index, but are characterized by remarkable differences in the molecular conformation. The straight stacking of molecular beta-strands present in the beta-sheet structure of $(VGGVG)_3$ may trigger the formation of regular fibrils offering a surface where cells anchor themselves in a friendly environment more suitable for their survival.

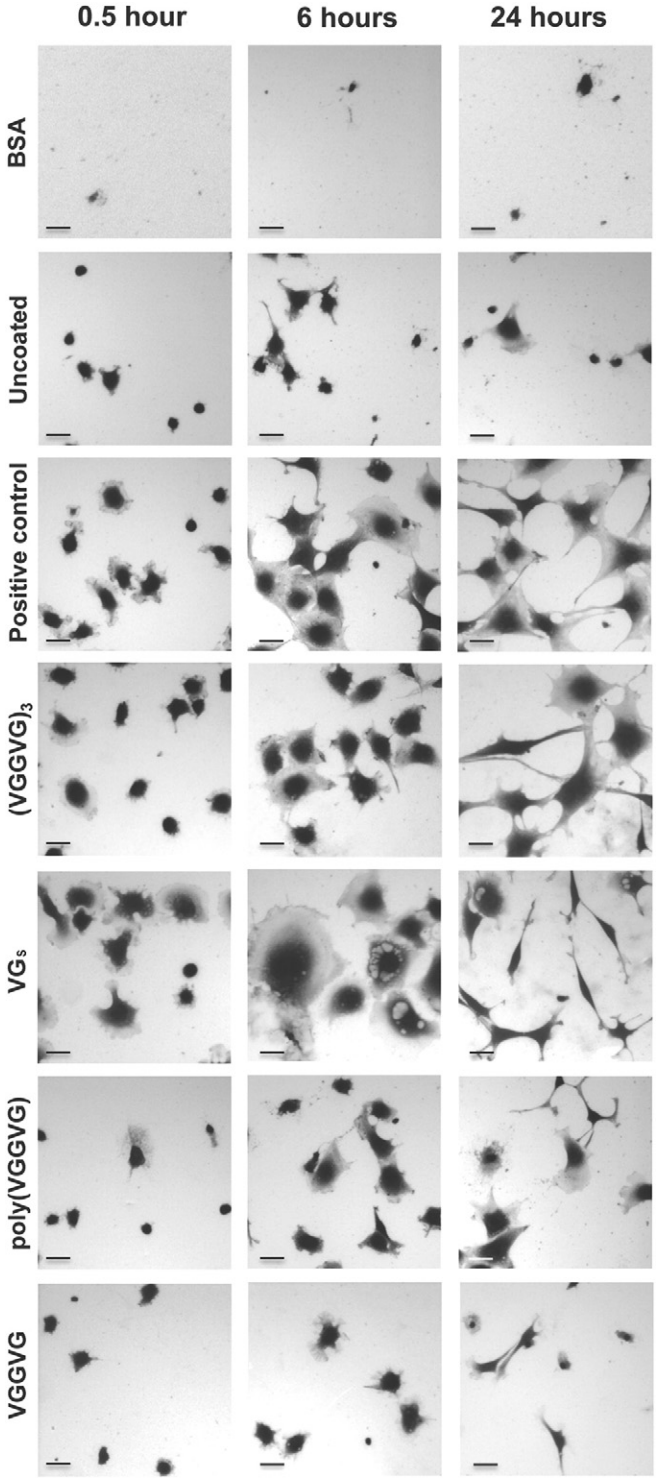

Fig. 10. Spreading of 3T3 fibroblasts. Cells were cultured in the absence of serum on bacteriologic Petri dishes coated with 100 μg/ml of $(VGGVG)_3$, poly(VGGVG), VGGVG and the VGs scrambled peptide. Dishes uncoated or coated with BSA (negative control) or tissue culture dishes (positive control) were taken as additional reference parameters. Morphology was evaluated by phase contrast microscopy after 0.5, 6 and 24 h from seeding. Images are representative of at least two experiments. Bars = 50 μm.

These data let us distinguish between general effects of hydrophobic peptides versus the specific sequences that are being tested and further support the concept that amyloid-like fibrils are not toxic per se and that hydropathy can favor cell attachment, but the fibrillar structure has a stronger effect on cell spreading, suggesting that the specific

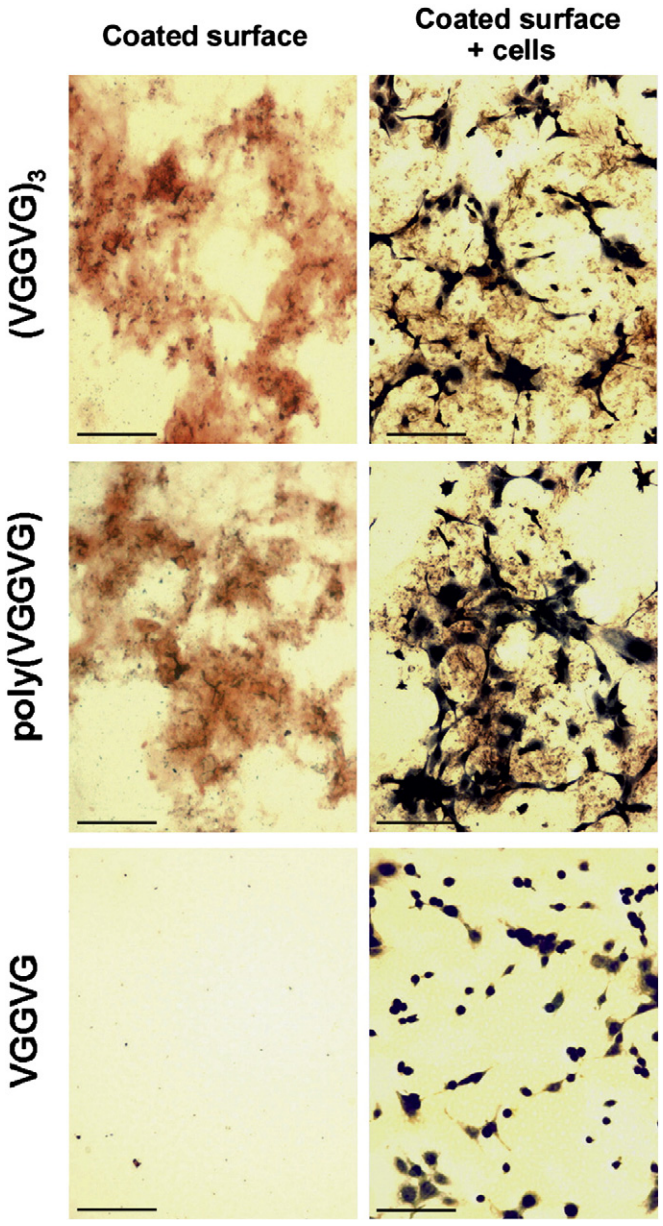

Fig. 11. Cell distribution on ELPs. 3T3 fibroblasts, grown for 24 h in the absence of serum on surfaces coated with amyloid-like fibrils (Congo red positive), were stained with ferric-hematoxylin and observed by phase contrast microscopy. Amyloid-like fibrils can be clearly visualized by their positivity to CR staining both in the absence (left panels) or in the presence of 3 T3 fibroblasts (right panels). Images are representative of two experiments. Bars = 100 μm.

surface topography can play a role in cellular responses (Yoshiike et al., 2007; Gras et al., 2008; Ohga et al., 2009; Cinar et al., 2012).

Finally, the co-staining with Congo red and ferric-haematoxylin of amyloid-like fibrils and cells, respectively, indicates that cells specifically interact with ELPs, rather than with uncoated areas of Petri dishes, as demonstrated with other matrix-coated surfaces (Boraldi et al., 2003), further supporting the potential use of $(VGGVG)_3$ for biomaterial applications.

In conclusion, this study provides a structural and a biological characterization of $(VGGVG)_3$, a peptide of monodispersed molecular weight that is able to self-assemble into short amyloid-like fibrils. Moreover, these fibrils are not cytotoxic and provide a good substrate for both cell attachment and spreading. These findings are in agreement with the large body of data indicating that amyloid-like fibrils can be used as potential nanostructures for their weaker or absent toxicity, for their ability to efficiently interact with cells, for their stability and low cost of production, in addition to the possibility to realize specifically functionalized coated surfaces.

4. Experimental procedures

4.1. Polypeptide synthesis and purification

The $(VGGVG)_3$ peptide and the scrambled peptide, VVVGGGGVGV GVGGG, were synthesized by solid phase peptide synthesis methodology on a Tribute automatic peptide synthesizer (Protein Technologies Inc., Tucson, AZ, USA). The synthesis scale was 0.25 mmol with Fmoc/HBTU chemistry. Fmoc-alfa-amino acids were purchased from Inbios (Pozzuoli, Italy). The polypeptide was cleaved from resin by an aqueous solution of 95% trifluoroacetic acid, lyophilized and purified by semi-preparative reversed-phase high-performance liquid chromatography (HPLC). A binary gradient was applied using H_2O (0.1% TFA) and CH_3CN (0.1% TFA) as solvents. Purity of the polypeptides was assessed by MALDI-TOF mass spectrometry.

The syntheses of the monomer VGGVG and of the poly(VGGVG) were performed as previously described (Flamia et al., 2004).

The scrambled peptide VGs was designed through the permutation of the original peptide sequence $(VGGVG)_3$ chosen out of complete randomness and generated by the on-line software tool RandSeq, available at the website http://web.expasy.org/randseq/.

4.2. Circular dichroism (CD) spectroscopy

Circular dichroism (CD) spectra were acquired with a JASCO J-815 Spectropolarimeter (JASCO, Milan, Italy) under constant nitrogen flush, using a HAAKE water bath with a temperature controller made of a cylindrical quartz cell of 0.1-cm path length. Spectra were acquired over a wavelength range of 190–250 nm at the indicated temperatures by taking points every 0.1 nm, with a scan speed of 20 nm per min, an integration time of 2 s, and a bandwidth of 1 nm. Samples at a concentration of 0.1 mg/ml in Milli-Q water were equilibrated for a few minutes prior to measurement at each temperature. CD spectra represented the average of 16 scans and all final spectra were obtained after subtracting the blank. Data are expressed in terms of [Θ] and the molar ellipticity in units of degree cm^2 $dmol^{-1}$. For the evaluation of secondary structure content, analysis of CD data was performed with DichroWeb analysis webserver using the CONTINLL algorithm (Whitmore and Wallace, 2008).

4.3. Nuclear magnetic resonance (NMR) spectroscopy

All NMR experiments were performed on a Varian Unity INOVA 500 MHz spectrometer (Varian medical systems, Palo Alto, CA, USA) equipped with a 5 mm triple-resonance probe and z-axial gradients. The purified peptide was dissolved at a concentration of 1 mM in 700 μl of H_2O/D_2O (90/10, v/v) containing 0.1 mM of 3-(trimethylsily1)-1-propane sulfonic acid (DSS) as internal reference standard at 0 ppm or at a concentration of 2 mM in 700 μl of DMSO-d_6, containing TMS as internal referencing standard. One-dimensional spectra were acquired in Fourier mode with quadrature detection and the water signal was suppressed by double-pulsed field-gradient spin-echo (Hwang and Shaka, 1995). Two-dimensional Total Correlation Spectroscopy (TOCSY) (Davis and Bax, 1985) and ROESY (Jeener et al., 1979) spectra were collected in the phase-sensitive mode using the States method. Typical data were 2048 complex data points, 32 or 64 transients and 256 increments. Relaxation delays were set to 2.5 s and spinlock (MLEV-17) mixing time was 80 ms for TOCSY while 200–300 ms mixing time was applied to ROESY experiments. Shifted sine bell squared

weighting and zero filling to 2 K × 2 K was applied before Fourier transform. Amide proton temperature coefficients were usually measured from 1D ^{1}H NMR spectra recorded in 5 °C increments from 20 °C to 45 °C. Data were processed with VNMRJ 2.2D. ^{1}H sequential resonance assignments were made by the approach described by Wüthrich (Wüthrich, 1986).

4.4. Fourier transform infrared (FTIR) spectroscopy

The $(VGGVG)_3$ polypeptide was analyzed by FTIR either as a lyophilized powder or as fibrils in KBr pellets (1 mg/100 mg), as previously described (Salvi et al., 2013). Spectra were recorded on a Jasco FT-IR-460 PLUS spectrophotometer in the range 400–4000 cm^{-1} at ambient temperature. Each recorded spectrum (average of 90 scans) was collected at a spectral resolution of 2 cm^{-1} and then smoothed by using the Savitzky–Golay algorithm. The decomposition of FTIR spectra was performed using the peak fitting module implemented in the Origin© software (Microcalc Inc.,Waltham, MA, USA) based on the second derivative method. In the curve fitting procedure, the Gaussian peak shape has been used for all peaks.

4.5. Thioflavin-T (ThT) fluorescence spectroscopy

The time course of the aggregation process of the polypeptides was monitored using the fluorescent dye, ThT (LeVine, 1999; Nilsson, 2004) with a few modifications. ThT stock solution (2.5 mM in Tris buffer 50 mM, NaCl 1.5 M, $CaCl_2$ 1 mM, pH 7.0) was filtered through a 0.22 μm syringe filter and diluted into the Tris buffer (1 ml to 50 ml) to generate the working solution (50 μM). The polypeptides were solubilized in Milli-Q water or 50% DMSO/water solution to yield a final concentration of 1 mg/ml and then incubated at 37 °C for more than 24 h. The extent of aggregation was assessed, at intervals of 1, 3, 6, 12, 24 h, by removing 250 μl of each polypeptide from the incubated samples and by adding 250 μl of ThT working solution to a final volume of 500 μl. Fluorescence intensity was monitored at 450 nm excitation and 482 nm emission, after briefly vortexing the mixture in the dark, using an LS-50b spectrofluorimeter (PerkinElmer, Waltham, MA, USA) into a 1 cm path length quartz cuvette. Fluorescence intensity for diluted ThT solution was measured and subtracted from sample intensities. Data from three identical samples in separate experiments were then averaged to provide the final values.

4.6. Congo red (CR) spectroscopic assay

Congo red (CR) binding experiments were performed as previously described (Salvi et al., 2011) using 550 μl aliquots of a suspension made of 1 mg/ml of the peptide (incubated 1 h and 24 h at 37 °C) mixed with 50 μl of solution containing 0.25 mM CR, in Milli-Q water. After about 30 min incubation period, the binding was measured spectrophotometrically at 540 nm (Nilsson, 2004). These measurements were collected together with negative control solutions of dye in the absence of polypeptide and of polypeptide sample in the absence of dye. The value of polypeptide alone was subtracted from the value of CR with polypeptide to correct the turbidity of the sample due to the aggregated material. The intensity values from three identical samples in separate experiments were then averaged and plotted.

4.7. Atomic force microscopy (AFM)

At fixed times during incubation, 10 μl aliquot of each sample was deposited on silicon (100) wafer substrates (Aldrich, St. Louis, MO, USA). After air-drying, AFM observations were carried out by using the XE-120 microscope (Park Systems) at room temperature in intermittent contact mode. Scan rates were between 0.2 and 1.5 Hz, using ultrasharp rectangular Si cantilevers (NCHR, Park Systems, Suwon, Korea) (tip radius less than 5 nm) with the nominal resonance frequency and force constant of 330 kHz and 42 N/m, respectively, or diamond tips (SCD, Mikromasch) with typical spike curvature radius less than 7 nm, nominal resonance frequency of 325 kHz and typical force constant 46 N/m. Phase imaging is based on the variation of the cantilever phase oscillation during the Tapping mode scan and provides information on surface properties not revealed by topography imaging.

4.8. Transmission electron microscopy (TEM)

ELPs and the VGs peptide (1 mg/ml) were diluted in Milli-Q water at a final concentration of 10 μg/ml and incubated for 24 h at 37 °C. Negative staining was performed by applying 10 μl of each sample onto a formvar- and carbon-coated copper grids. Few drops of 1% uranyl acetate in distilled water were used to increase the contrast and the electron density of the samples. After air drying, grids were observed by transmission electron microscopy (Jeol JEM 1200EX, Jeol, Tokyo, Japan) at 80 keV.

4.9. Cell culture and treatments

Mouse fibroblast cells (3T3) were routinely cultured in Dulbecco's Modified Eagle Medium (DMEM) supplemented with 10% Foetal Bovine Serum (Australian FBS, Gibco, Invitrogen Corporation, NY, USA), 100 U/ml penicillin, 100 μg/ml streptomycin (Invitrogen). Once amplified, cells were cultured in the presence of $(VGGVG)_3$ as well as of VGGVG and poly(VGGVG), taken as negative and positive control of amyloidogenic peptides, respectively.

To form fibrillar preparations, 1 mg of each peptide was resuspended in 1 ml of dH_2O and incubated for 24 h at 37 °C and then left at room temperature until use.

4.10. Cell proliferation

1.0×10^4 cells were cultured into 35 mm Petri dishes in 2 ml DMEM containing 10% FBS. Cells were grown in the presence of 0, 10, 100, 250, 500 μg/ml of ELPs that were added to cells after 8 h from seeding, in order to avoid any effect on cell attachment.

Medium was replaced daily with DMEM supplemented with different concentrations of ELPs. After 24, 48, 72 and 96 h, cells were detached by 0.25% trypsin-EDTA for 10 min, centrifuged, suspended in a small amount of medium and counted by the Neubauer chamber. Experiments were always performed in triplicate and were repeated twice.

A set of experiments was performed forcing ELPs to remain in a non-fibrillar state by the presence of DMSO. However, cell proliferation was assessed only at low doses of ELPs (up to 10 μg/ml) since the amount of DMSO used to dissociate the peptides was cytotoxic and therefore these experimental conditions were no further used.

4.11. FACS analysis

ROS analysis was performed on proliferating cells as previously described (Boraldi et al., 2009). Briefly, after 1 hour incubation with ELPs (0, 10, 100, 250 and 500 μg/ml), cells were stained with dihydroethidium (DH_2, 1 mM) and 2′,7′-dichlorodihydrofluorescein diacetate (H_2DCF-DA, 2 mM) probes (Molecular Probes, Eugene, OR) for the determination of superoxide anion ($O_2^{-\bullet}$) and hydrogen peroxide (H_2O_2), respectively. Cells were analyzed on an EPICS XL flow cytometer (Beckman Coulter, Milan, Italy) at the emission wavelength of 575 and 520 nm. Ten thousand events were collected and evaluated for each treatment using a WINMDI 2.8 program. Experiments were performed in duplicate and repeated twice.

4.12. Attachment and spreading assay

Bacteriologic Petri plates (35 mm in diameter), either uncoated or coated with 1 ml bovine serum albumin (BSA) (1% in dH_2O) or with 1 ml of ELPs or of the VGs peptide (100 μg in dH_2O), were used. Tissue culture plates were taken as a positive control of cell attachment and spreading, since the hydrophilic charges of the polystyrene surface are known to induce optimal cell attachment. Surface coating was obtained by covering dishes with 1 ml of BSA, ELPs or VGs peptide. Solutions were left to dry overnight at room temperature under sterile conditions. Before use, dishes were washed twice with phosphate buffered solution (PBS). A set of ELPs-coated dishes was preliminarily evaluated by staining with Congo red in dH_2O for 20 min in order to assess that the procedure lead to successful biopolymer deposition on the surface as well as formation of stable amyloid-like fibrils. An aliquot of 2.5×10^5 cells in 2 ml of serum-free DMEM was added to each dish and allowed to attach for 0.5, 1, 3 and 6 h at 37 °C. At each time point, still floating cells were removed with the medium, whereas attached cells were fixed in 3% paraformaldehyde in PBS for 10 min, washed in PBS, stained with crystal violet (0.5% in 20% methanol) for 15 min and extensively washed with distilled water. The colour retained by cells was then eluted by 0.1 M sodium citrate in 50% ethanol (pH 4.2) for 30 min at room temperature and read in a spectrophotometer at 540 nm, optical density (OD) being proportional to the number of adherent cells (Quaglino et al., 1997). OD values in each experimental condition were related to the highest value obtained by the positive control set at 100%.

Cell spreading was evaluated with a phase contrast light microscope (Zeiss axiophot, Carl Zeiss, Jena, Germany) up to 24 h from seeding.

Moreover, in order to evaluate 3T3 distribution on amyloid fibrils, after 24 h from cell seeding, coated plates were fixed in 3% paraformaldehyde in PBS for 10 min, stained with ferric haematoxylin for 15 min, washed with dH_2O and further stained for 30 min with a saturating solution of CR (80% EtOH: 20% dH_2O) (Nilsson, 2004). Samples were allowed to dry at room temperature and observed with a Zeiss axiophot optical microscope.

All experiments were performed in triplicate and repeated twice.

Acknowledgments

This work was supported by MIUR (PRIN 2010-Project 2010L) (SH3K).

References

Barth, A., 2007. Infrared spectroscopy of proteins. Biochim. Biophys. Acta 176, 1073–1101.
Bellingham, C.M., Lillie, M.A., Gosline, J.M., Wright, G.M., Starcher, B.C., Bailey, A.J., et al., 2003. Recombinant human elastin polypeptides self-assemble into biomaterials with elastin-like properties. Biopolymers 70, 445–455.
Boraldi, F., Croce, M.A., Quaglino, D., Sammarco, R., Carnevali, E., Tiozzo, R., et al., 2003. Cell-matrix interactions of in vitro human skin fibroblasts upon addition of hyaluronan. Tissue Cell 35, 37–45.
Boraldi, F., Annovi, G., Guerra, D., Paolinelli-Devincenzi, C., Garcia-Fernandez, M.I., Panico, F., et al., 2009. Fibroblast protein profile analysis highlights the role of oxidative stress and vitamin K recycling in the pathogenesis of pseudoxanthoma elasticum. Proteomics Clin. Appl. 3, 1084–1098.
Bucciantini, M., Giannoni, E., Chiti, F., Baroni, F., Formigli, L., Zurdo, J., et al., 2002. Inherent toxicity of aggregates implies a common mechanism for protein misfolding diseases. Nature 416, 507–511.
Bucciantini, M., Calloni, G., Chiti, F., Formigli, L., Nosi, D., Dobson, C.M., et al., 2004. Prefibrillar amyloid protein aggregates share common features of cytotoxicity. J. Biol. Chem. 279, 31374–31382.
Butterfield, D.A., Drake, J., Pocernich, C., Castegna, A., 2001. Evidence of oxidative damage in Alzheimer's disease brain: central role for amyloid beta-peptide. Trends Mol. Med. 7, 548–554.
Caughey, B., Lansbury, P.T., 2003. Protofibrils, pores, fibrils, and neurodegeneration: separating the responsible protein aggregates from the innocent bystanders. Annu. Rev. Neurosci. 26, 267–298.
Cecchi, C., Fiorillo, C., Baglioni, S., Pensalfini, A., Bagnoli, S., Nacmias, B., et al., 2007. Increased susceptibility to amyloid toxicity in familial Alzheimer's fibroblasts. Neurobiol. Aging 28, 863–876.
Channon, K., MacPhee, C.E., 2008. Possibilities for 'smart' materials exploiting the self-assembly of polypeptides into fibrils. Soft Matter 4, 647–652.
Cherny, I., Gazit, E., 2008. Amyloids: not only pathological agents but also ordered nanomaterials. Angew. Chem. Int. Ed. Engl. 47, 4062–4069.
Cinar, G., Ceylan, H., Urel, M., Erkal, T.S., Deniz-Tekin, E., Tekinay, A.B.., et al., 2012. Amyloid inspired self-assembled peptide nanofibers. Biomacromolecules 13, 3377–3387.
Cleary, J.P., Walsh, D.M., Hofmeister, J.J., Shankar, G.M., Kuskowski, M.A., Selkoe, D.J., et al., 2005. Natural oligomers of the amyloid-beta protein specifically disrupt cognitive function. Nat. Neurosci. 8, 79–84.
Davis, D.G., Bax, A., 1985. MLEV-17-based two-dimensional homonuclear magnetization transfer spectroscopy. J. Am. Chem. Soc. 10, 2820–2821.
Del Mercato, L.L., Maruccio, G., Pompa, P.P., Bochicchio, B., Tamburro, A.M., Cingolani, R., et al., 2008. Amyloid-like fibrils in elastin-related polypeptides: structural characterization and elastic properties. Biomacromolecules 9, 796–803.
Dobson, C.M., 1999. Protein misfolding, evolution and disease. Trends Biochem. Sci. 24, 329–332.
Flamia, R., Zhdan, P.A., Martino, M., Castle, J.E., Tamburro, A.M., 2004. AFM study of the elastin-like biopolymer poly(ValGlyGlyValGly). Biomacromolecules 5, 1511–1518.
Flamia, R., Lanza, G., Salvi, A.M., Castle, J.E., Tamburro, A.M., 2005. Conformational study and hydrogen bonds detection on elastin-related polypeptides using X-ray photoelectron spectroscopy. Biomacromolecules 6, 1299–1309.
Flamia, R., Salvi, A.M., D'Alessio, L., Castle, J.E., Tamburro, A.M., 2007. Transformation of amyloid-like fibers, formed from an elastin-based biopolymer, into a hydrogel: an X-ray photoelectron spectroscopy and atomic force microscopy study. Biomacromolecules 8, 128–138.
Gharibyan, A.L., Zamotin, V., Yanamandra, K., Moskaleva, O.S., Margulis, B.A., Kostanyan, I. A., et al., 2007. Lysozyme amyloid oligomers and fibrils induce cellular death via different apoptotic/necrotic pathways. J. Mol. Biol. 365, 1337–1349.
Gras, S.L., Tickler, A.K., Squires, A.M., Devlin, G.L., Horton, M.A., Dobson, C.M., et al., 2008. Functionalised amyloid fibrils for roles in cell adhesion. Biomaterials 29, 1553–1562.
Hwang, T.L., Shaka, A.J., 1995. Water suppression that works. Excitation sculpting using arbitrary waveforms and pulsed field gradients. J. Magn. Reson. Ser. 112, 275–279.
Jeener, J., Meier, B.H., Bachmann, P., Ernst, R.R., 1979. Investigation of exchange processes by two-dimensional NMR spectroscopy. J. Chem. Phys. 71, 4546–4553.
Kayed, R., Head, E., Thompson, J.L., McIntire, T.M., Milton, S.C., Cotman, C.W., et al., 2003. Common structure of soluble amyloid oligomers implies common mechanism of pathogenesis. Science 300, 486–489.
Kelly, J.W., 1998. The alternative conformations of amyloidogenic proteins and their multi-step assembly pathways. Curr. Opin. Struct. Biol. 8, 101–106.
Krimm, S., Bandekar, J., 1986. Vibrational spectroscopy and conformation of peptides, polypeptides, and proteins. Adv. Protein Chem. 38, 181–364.
Kyte, J., Doolittle, R.F., 1982. A simple method for displaying the hydropathic character of a protein. J. Mol. Biol. 157, 105–132.
Lashuel, H.A., Labrenz, S.R., Woo, L., Serpell, L.C., Kelly, J.W., 2000. Protofilaments, filaments, ribbons, and fibrils from peptidomimetic self-assembly: implications for amyloid fibril formation and materials science. J. Am. Chem. Soc. 122, 5262–5277.
LeVine III, H., 1999. Quantification of beta-sheet amyloid fibril structures with thioflavin T. Methods Enzymol. 309, 274–284.
Loksztejn, A., Dzwolak, W., 2009. Noncooperative dimethyl sulfoxide-induced dissection of insulin fibrils: toward soluble building blocks of amyloid. Biochemistry 48, 4846–4851.
MacPhee, C.E., Dobson, C.M., 2000. Formation of mixed fibrils demonstrates the generic nature and potential utility of amyloid nanostructures. J. Am. Chem. Soc. 122, 12707–12713.
Mankar, S., Anoop, A., Sen, S., Maji, S.K., 2011. Nanomaterials: amyloids reflect their brighter side. Nano Rev. 2. http://dx.doi.org/10.3402/nano.v2i0.6032.
Manning, M.C., Illangasekare, M., Woody, R.W., 1988. Circular dichroism studies of distorted alpha-helices, twisted beta-sheets, and beta turns. Biophys. Chem. 31, 77–86.
Martino, M., Bavoso, A., Guantieri, V., Coviello, A., Tamburro, A.M., 2000. On the occurrence of polyproline II structure in elastin. J. Mol. Struct. 519, 173–189.
Nilsson, M.R., 2004. Techniques to study amyloid fibril formation in vitro. Methods 34, 151–160.
Novitskaya, V., Bocharova, O.V., Bronstein, I., Baskakov, I.V., 2006. Amyloid fibrils of mammalian prion protein are highly toxic to cultured cells and primary neurons. J. Biol. Chem. 281, 13828–13836.
Ohga, Y., Katagiri, F., Takeyama, K., Hozumi, K., Kikkawa, Y., Nishi, N., et al., 2009. Design and activity of multifunctional fibrils using receptor-specific small peptides. Biomaterials 30, 6731–6738.
Pieri, L., Madiona, K., Bousset, L., Melki, R., 2012. Fibrillar α-synuclein and huntingtin exon 1 assemblies are toxic to the cells. Biophys. J. 102, 2894–2905.
Provencher, S.W., Glockner, J., 1981. Estimation of globular protein secondary structure from circular dichroism. Biochemistry 20, 33–37.
Quaglino, D., Bergamini, G., Croce, A., Boraldi, F., Barbieri, D., Caroli, A., et al., 1997. Cell behavior and cell-matrix interactions of human palmar aponeurotic cells in vitro. J. Cell. Physiol. 173, 415–422.
Quaglino, D., Guerra, D., Pasquali-Ronchetti, I., 2009. Elastin and elastin-based polymers. In: Hussain, F. (Ed.), Nano and biocomposites. Taylor & Francis, pp. 249–274.
Rodriguez-Cabello, J.C., 2004. Smart elastin-like polymers. Adv. Exp. Med. Biol. 553, 45–57.
Salvi, A.M., Moscarelli, P., Satriano, G., Bochicchio, B., Castle, J.E., 2011. Influence of amino acid specificities on the molecular and supramolecular organization of glycine-rich elastin-like polypeptides in water. Biopolymers 95, 702–721.
Salvi, A.M., Moscarelli, P., Bochicchio, B., Lanza, G., Castle, J.E., 2013. Combined effects of solvation and aggregation propensity on the final supramolecular structures adopted by hydrophobic, glycine-rich, elastin-like polypeptides. Biopolymers 99, 292–313.
Sörgjerd, K., Klingstedt, T., Lindgren, M., Kågedal, K., Hammarström, P., 2008. Prefibrillar transthyretin oligomers and cold stored native tetrameric transthyretin are cytotoxic in cell culture. Biochem. Biophys. Res. Commun. 377, 1072–1078.

Sunde, M., Serpell, L.C., Bartlam, M., Fraser, P.E., Pepys, M.B., Blake, C.C.F., 1997. Common core structure of amyloid fibrils by synchrotron X-ray diffraction. J. Mol. Biol. 273, 729–739.
Surewicz, W.K., Mantsch, H.H., Chapman, D., 1993. Determination of protein secondary structure by Fourier transform infrared spectroscopy: a critical assessment. Biochemistry 32, 389–394.
Tabner, B.J., El-Agnaf, O.M., German, M.J., Fullwood, N.J., Allsop, D., 2005. Protein aggregation, metals and oxidative stress in neurodegenerative diseases. Biochem. Soc. Trans. 33, 1082–1086.
Tamburro, A.M., Bochicchio, B., Pepe, A., 2003. Dissection of human tropoelastin: exon-by-exon chemical synthesis and related conformational studies. Biochemistry 42, 13347–13362.
Tamburro, A.M., Pepe, A., Bochicchio, B., Quaglino, D., Pasquali-Ronchetti, I., 2005. Supramolecular amyloid-like assembly of the polypeptide sequence coded by exon 30 of human tropoelastin. J. Biol. Chem. 280, 2682–2690.
Tamburro, A.M., Lorusso, M., Ibris, N., Pepe, A., Bochicchio, B., 2010. Investigating by circular dichroism some amyloidogenic elastin-derived polypeptides. Chirality 22 (Suppl. 1), E56–E66.
Tofoleanu, F., Buchete, N.V., 2012. Alzheimer Aβ peptide interactions with lipid membranes. Prion 6, 339–345.
Trabbic-Carlson, K., Setton, L.A., Chilkoti, A., 2003. Swelling and mechanical behaviors of chemically cross-linked hydrogels of elastin-like polypeptides. Biomacromolecules 4, 572–580.
Whitmore, L., Wallace, B.A., 2008. Protein secondary structure analyses from circular dichroism spectroscopy: methods and reference databases. Biopolymers 89, 392–400.
Wishart, D.S., Sykes, B.D., Richards, F.M., 1992. The chemical shift index: a fast and simple method for the assignment of protein secondary structure through NMR spectroscopy. Biochemistry 31, 1647–1651.
Wüthrich, K., 1986. NMR of proteins and nucleic acids. Wiley, New York.
Yoshiike, Y., Akagi, T., Takashima, A., 2007. Surface structure of amyloid-beta fibrils contributes to cytotoxicity. Biochemistry 46, 9805–9812.
Zandomeneghi, G., Krebs, M.R., McCammon, M.G., Fändrich, M., 2004. FTIR reveals structural differences between native beta-sheet proteins and amyloid fibrils. Protein Sci. 13, 3314–3321.